


 Cite this: *RSC Adv.*, 2025, 15, 22154

# Improving the luminescence properties of the near-infrared phosphor $\text{Ca}_{0.8}\text{Sr}_{0.2}\text{O}:\text{Eu}^{2+}$ via energy transfer and its application in the concentration detection of ethanol solutions†

 Yuxuan Liang,<sup>a</sup> Pengfei Du,<sup>b</sup> Yanhong Wei,<sup>c</sup> Xurui Hu,<sup>\*b</sup> Xiaojie Li,<sup>a</sup> Zhijun Wang,<sup>id a</sup> Jie Gong,<sup>a</sup> Mengdi Liu,<sup>a</sup> Panlai Li<sup>id a</sup> and Wenge Ding<sup>\*a</sup>

In this work, a near-infrared (NIR) phosphor  $\text{Ca}_{0.8}\text{Sr}_{0.2}\text{O}:\text{Eu}^{2+}$  was prepared via a solid-state method, and its luminescence properties were improved by co-doping with  $\text{Ce}^{3+}$  ions. The decay curves of  $\text{Ca}_{0.8}\text{Sr}_{0.2}\text{O}:\text{Ce}^{3+}$ ,  $\text{Eu}^{2+}$  confirmed that there was an obvious energy transfer from  $\text{Ce}^{3+}$  to  $\text{Eu}^{2+}$ , which enhanced the quantum efficiency of  $\text{Ca}_{0.8}\text{Sr}_{0.2}\text{O}:\text{Eu}^{2+}$ . The thermal stability can also be enhanced by introducing Ce, which reduces the probability of non-radiative transitions at elevated temperatures, thereby minimizing electron loss. An NIR light emitting diode (LED) was fabricated by combining a blue LED chip with  $\text{Ca}_{0.8}\text{Sr}_{0.2}\text{O}:\text{Ce}^{3+}$ ,  $\text{Eu}^{2+}$ , which was applied for the concentration detection of ethanol solutions.

Received 8th April 2025

Accepted 4th June 2025

DOI: 10.1039/d5ra02418h

[rsc.li/rsc-advances](https://rsc.li/rsc-advances)

## 1. Introduction

In recent years, near-infrared (NIR) light has found widespread application in fields such as night vision, biological tissue penetration, solution detection, food quality detection, and plant growth. This is because NIR light possesses several advantageous properties: it has strong penetration capability, causes minimal damage to the human body, is invisible to the human eye, and overlaps with certain organic functional groups like C–H ( $2980\text{ cm}^{-1}$ ) and C–O ( $1100\text{ cm}^{-1}$ ).<sup>1–9</sup> As the core component for these applications, the NIR light source needs to meet the conditions of broadband emission, good stability, miniaturization and fast response.<sup>10</sup> Traditional NIR light sources (such as the halogen tungsten lamp) can emit wide-range NIR light; however, they have the disadvantages of high energy consumption, large volume and short life, which cannot meet the requirements for practical use.<sup>11,12</sup> NIR LED is another NIR light source, which is made up of a combination of multiple NIR LEDs of different wavelengths arranged in an array to meet the demand of a broadband NIR light source. Although this NIR

light source exhibits a long life and high efficiency, its large volume and the emission of various spectra by different LEDs consistently affect the overall spectral type of the light source with changes in temperature and time. These deficiencies make NIR LEDs unable to meet practical requirements. Currently, NIR phosphor conversion LEDs are considered ideal NIR light sources to satisfy the practical demands of the above-mentioned fields owing to their small size, long life and fast response.<sup>13–15</sup> The main preparation method of an NIR pc-LED involves coating the broadband NIR phosphor onto a mature blue LED; hence, it is crucial to explore efficient broadband NIR phosphors.

Currently, NIR phosphors can be obtained by doping with the following ions: trivalent rare-earth ions ( $\text{Pr}^{3+}$ ,  $\text{Yb}^{3+}$ ,  $\text{Nd}^{3+}$ ), transition metal ions ( $\text{Mn}^{4+}$ ,  $\text{Ni}^{2+}$ ,  $\text{Cr}^{3+}$ ), and divalent rare-earth ions ( $\text{Eu}^{2+}$ ). Because electronic transitions inside the f–f electronic configuration of trivalent rare earth ions is forbidden and has a weak absorption capacity, such materials exhibit low luminous efficiency and a narrow emission bandwidth, which cannot meet the requirements of efficient wide-band NIR light sources, limiting their applications.  $\text{Mn}^{4+}$  ions tend to occupy a strong crystal field environment. They usually exhibit narrow band emissions, and the spectrum is not easy to regulate, thus lacking the requirements for a broadband emission NIR light source. Although the emission wavelength of  $\text{Ni}^{2+}$  ions is greater than 1000 nm, their luminescence efficiency is low with a relatively poor thermal stability, and it cannot be effectively applied as an NIR light source.  $\text{Cr}^{3+}$  exhibits a broadband NIR emission at  ${}^4\text{T}_2 \rightarrow {}^4\text{A}_2$  level transition. This transition is outside the 3d electron layer, and hence, it is vulnerable to the influence of

<sup>a</sup>National-Local Joint Engineering Laboratory of New Energy Photoelectric Devices, Hebei Key Laboratory of Optic-electronic Information and Materials, College of Physics Science & Technology, Hebei University, Baoding 071002, China. E-mail: [dwg@hbu.edu.cn](mailto:dwg@hbu.edu.cn)

<sup>b</sup>School of Physical Science and Technology, Ningbo University, Ningbo 315211, China. E-mail: [huxurui@nbu.edu.cn](mailto:huxurui@nbu.edu.cn)

<sup>c</sup>Working Committee for the Care of the Next Generation, Hebei University, Baoding 071002, China

† Electronic supplementary information (ESI) available. See DOI: <https://doi.org/10.1039/d5ra02418h>





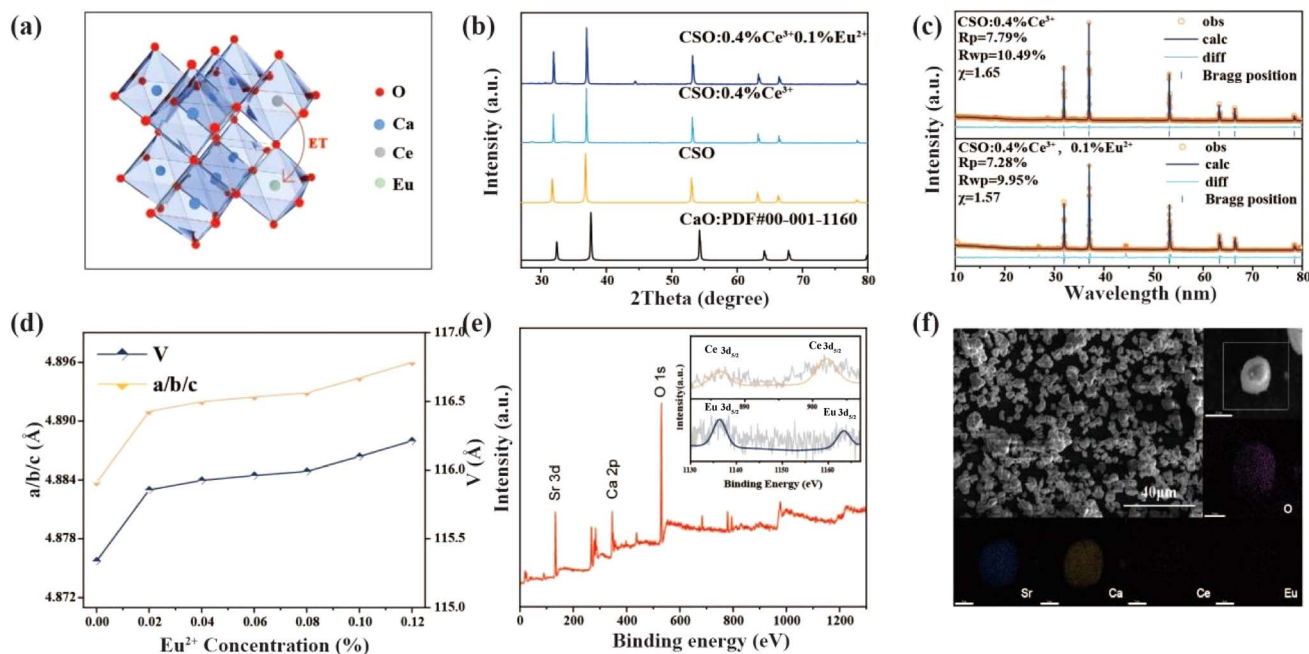


Fig. 1 (a) Crystal structure of CaO; (b) XRD patterns of  $\text{Ca}_{0.8}\text{Sr}_{0.2}\text{O}$ ,  $\text{Ca}_{0.8}\text{Sr}_{0.196}\text{O}(\text{CSO}):0.4\% \text{Ce}^{3+}$  and  $\text{CSO}:0.4\% \text{Ce}^{3+}, 0.1\% \text{Eu}^{2+}$ ; (c) rietveld refinement of  $\text{CSO}:0.4\% \text{Ce}^{3+}$  and  $\text{CSO}:0.4\% \text{Ce}^{3+}, 0.1\% \text{Eu}^{2+}$ ; (d) lattice parameters  $a/b/c$  and  $V$  with  $\text{Eu}^{2+}$  concentration; (e) XPS full survey spectrum of  $\text{CSO}:0.4\% \text{Ce}^{3+}, 0.1\% \text{Eu}^{2+}$ , inset: high-resolution XPS of  $\text{Ce}^{3+}$  and  $\text{Eu}^{2+}$ ; and (f) SEM and element mapping images of  $\text{CSO}:0.4\% \text{Ce}^{3+}, 0.1\% \text{Eu}^{2+}$ .

Table 1 Crystal cell parameters for  $\text{Ca}_{0.8}\text{Sr}_{0.2}\text{O}:0.4\% \text{Ce}^{3+}, y\text{Eu}^{2+}$  ( $y = 0-0.12\%$ ) obtained via refinement

| $y(\text{Eu}^{2+})$ | Cell parameters ( $\text{\AA}^3$ ) | Cell volume ( $\text{\AA}^3$ ) | $R_{\text{wp}}$ (%), $R_p$ (%), $\chi^2$ |
|---------------------|------------------------------------|--------------------------------|--|
| 0%                  | $a/b/c = 4.87572$                  | 115.909                        | 12.38, 8.5, 1.97                         |
| 0.02%               | $a/b/c = 4.88299$                  | 116.428                        | 14.59, 10.13, 2.08                       |
| 0.04%               | $a/b/c = 4.88396$                  | 116.498                        | 13.84, 9.8, 1.97                         |
| 0.06%               | $a/b/c = 4.88446$                  | 116.533                        | 12.56, 9.23, 1.76                        |
| 0.08%               | $a/b/c = 4.88488$                  | 116.563                        | 9.39, 6.79, 1.59                         |
| 0.1%                | $a/b/c = 4.88638$                  | 116.671                        | 9.95, 7.28, 1.57                         |
| 0.12%               | $a/b/c = 4.88797$                  | 116.785                        | 10.99, 9.8, 1.55                         |

samples exhibited fairly uniform particle sizes of approximately 10  $\mu\text{m}$ . Five elements, namely, Ca, Sr, O, Eu, and Ce were successfully identified.

### 3.2. Luminescence properties

Fig. 2(a) presents the emission spectrum of  $\text{CSO}:\text{Ce}^{3+}$  and the excitation spectrum of  $\text{CSO}:\text{Eu}^{2+}$ . The spectral overlap between 500 nm and 700 nm suggested the potential energy transfer from  $\text{Ce}^{3+}$  to  $\text{Eu}^{2+}$ . In order to further improve the  $\text{CSO}:\text{Ce}^{3+}$  performance by identifying the optimal  $\text{Ce}^{3+}$  concentration, the emission spectra of  $\text{CSO}:x\text{Ce}^{3+}$  ( $x = 0.1-1.3\%$ ) were investigated under a 467 nm excitation, and the optimal  $\text{Ce}^{3+}$  concentration was obtained as  $x = 0.4\%$  Fig. 2(b). Fig. 2(c) shows the emission spectra of  $\text{CSO}:0.4\% \text{Ce}^{3+}, y\text{Eu}^{2+}$  ( $y = 0-0.12\%$ ) under an excitation of 467 nm, and the NIR emission peak belonging to  $\text{Eu}^{2+}$  appeared at  $y = 0.06\%$ . Owing to concentration quenching, the NIR emission intensities first increased and then decreased as

the  $\text{Eu}^{2+}$  concentration gradually increased, and the maximum value appeared at  $y = 0.1\%$ . Fig. 2(d) presents the decay curves of  $\text{CSO}:0.4\% \text{Ce}^{3+}, y\text{Eu}^{2+}$  ( $y = 0-0.12\%$ ) at 581 nm, demonstrating the occurrence of energy transfer between  $\text{Ce}^{3+}-\text{Eu}^{2+}$ , and all the decay curves could be well fitted using the biexponential function as follows:<sup>16-18</sup>

$$I(t) = I_0 + A_1 \exp\left(-\frac{t}{\tau_1}\right) + A_2 \exp\left(-\frac{t}{\tau_2}\right) \quad (1)$$

where  $I(t)$  is the luminescence intensity,  $A_1$  and  $A_2$  are constants,  $\tau$  is the average lifetime, and  $\tau_1$  and  $\tau_2$  are the fast decay and slow decay lifetimes, respectively. The average lifetime  $\tau$  can be obtained using the following formula:<sup>19,20</sup>

$$\tau = (A_1\tau_1^2 + A_2\tau_2^2)/(A_1\tau_1 + A_2\tau_2) \quad (2)$$

The calculations showed that the average lifetimes of  $\text{Ce}^{3+}$  ions were 33.48 ns, 28.46 ns, 20.53 ns, 13.73 ns, 10.59 ns, 5.01 ns and 4.68 ns for  $y = 0\%, 0.02\%, 0.04\%, 0.06\%, 0.08\%, 0.10\%$ , and  $0.12\%$ , respectively. Clearly, the emission peak attributed to  $\text{Ce}^{3+}$  decreased monotonically with increasing  $\text{Eu}^{2+}$  concentration, proving the occurrence of energy transfer between  $\text{Ce}^{3+}-\text{Eu}^{2+}$ . Energy transfer efficiency is an important parameter, which can be calculated by the decrease in emission intensity using the following formula:<sup>21</sup>

$$\eta_T = 1 - I_s/I_{s0} \quad (3)$$

where  $I_{s0}$  and  $I_s$  represent the luminescence intensity of  $\text{Ce}^{3+}$  ions without and with  $\text{Eu}^{2+}$  ions, respectively, and  $\eta_T$  is the value



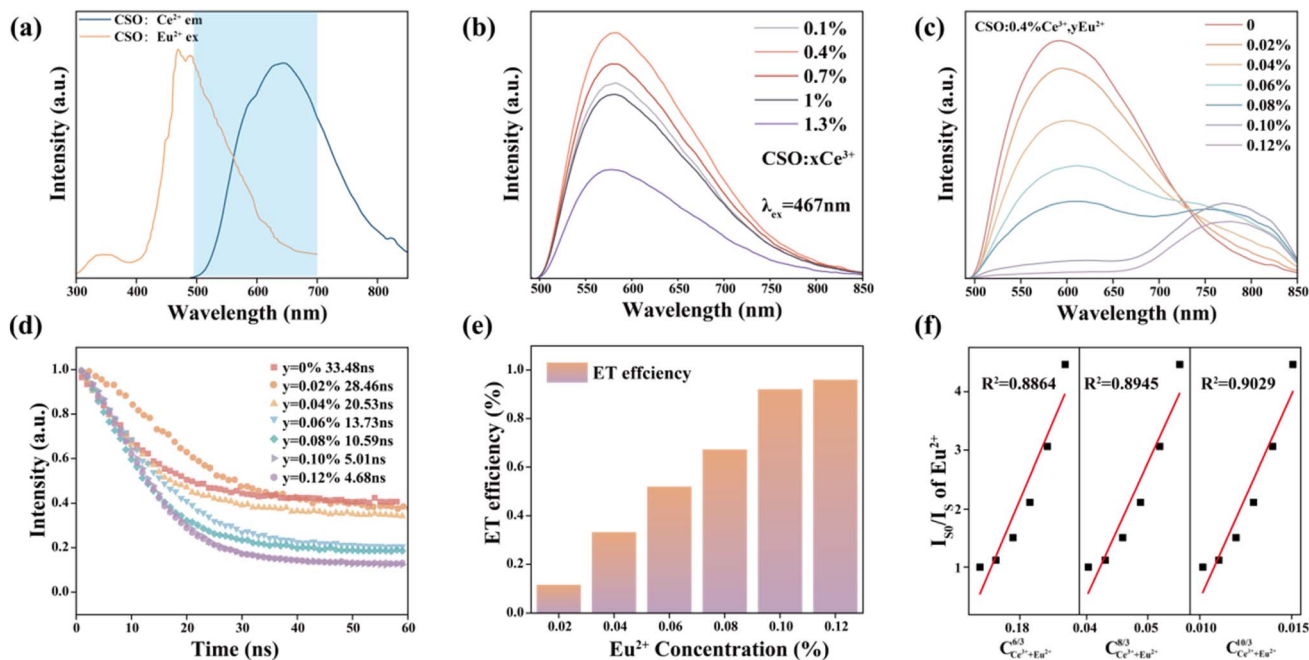


Fig. 2 (a) Emission spectrum of CSO:Ce<sup>3+</sup> and excitation spectrum of CSO:Eu<sup>2+</sup>; (b) emission spectra of CSO:Ce<sup>3+</sup> ( $x = 0.1-1.3\%$ ); (c) emission spectra of CSO:0.4% Ce<sup>3+</sup>,  $\gamma$ Eu<sup>2+</sup> ( $\gamma = 0-0.12\%$ ); (d) decay curves of CSO:0.4% Ce<sup>3+</sup>,  $\gamma$ Eu<sup>2+</sup> ( $\gamma = 0-0.12\%$ ); (e) energy transfer efficiency of CSO:0.4% Ce<sup>3+</sup>,  $\gamma$ Eu<sup>2+</sup> ( $\gamma = 0-0.12\%$ ) ( $\lambda_{\text{ex}} = 467 \text{ nm}$ ); and (f) dependence of  $(I_{\text{S0}}/I_{\text{S}})$  of Ce<sup>3+</sup> on  $C_{\text{Ce}^{3+}\text{+Eu}^{2+}}^{6/3}$ ,  $C_{\text{Ce}^{3+}\text{+Eu}^{2+}}^{8/3}$  and  $C_{\text{Ce}^{3+}\text{+Eu}^{2+}}^{10/3}$ .

of energy transfer efficiency. The calculated results are depicted in Fig. 2(e). The energy transfer efficiency reached a maximum of 96.6% at  $x = 0.12\%$ .

A concentration quenching phenomenon can arise from either electric multipolar interactions or exchange interactions. When the critical distance exceeds 0.5 nm, the electric multipolar interactions are likely to induce concentration quenching; conversely, at shorter distances, the exchange interactions tend to dominate.<sup>22</sup> As reported by Blaszczyk, the critical transfer distance ( $R_c$ ) can be expressed as:<sup>23</sup>

$$R_c = 2[3V/4\pi X_c N]^{1/3} \quad (4)$$

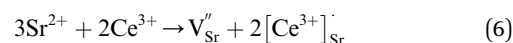
where  $N$  represents the number of host cations in the unit cell,  $V$  represents the volume per unit cell, and  $X_c$  represents the total critical concentration of Ce<sup>3+</sup> and Eu<sup>2+</sup> ions. For CSO substrate,  $V = 0.115909 \text{ nm}^3$ ,  $N = 14$ ,  $X_c = 0.005$ ; therefore,  $R_c$  is approximately 1.468 nm, which is significantly larger than 0.5 nm, indicating that the electric multipolar interaction caused a nonradiative concentration quenching of Ce<sup>3+</sup>-Eu<sup>2+</sup> ions. For electrical multipolar interactions, it may include the dipole-dipole (d-d), the dipole-quadrupole (d-q), and the quadrupole-quadrupole (q-q) interactions.<sup>24</sup> According to Dexter's energy transfer theory, the multipolar interaction<sup>24,25</sup> can be expressed using the linear relationship in the following formula:

$$\frac{\eta_0}{\eta_S} \propto C_{\text{S+A}}^{n/3} \quad (5)$$

where  $\eta_0$  and  $\eta_S$  are the energy transfer efficiency of Ce<sup>3+</sup> ions in the samples without and with Eu<sup>2+</sup> ions, respectively. The relative luminescence intensity ratio ( $I_{\text{S}}/I_{\text{S0}}$ ) can approximately

replace the ratio of  $\eta_0/\eta_S$ .  $C_{\text{S+A}}$  is the total concentration of Ce<sup>3+</sup> and Eu<sup>2+</sup> ions in the sample, and  $n = 6, 8, \text{ or } 10$ , indicating a d-d interaction, d-q interaction or q-q interaction, respectively. Fig. 2(f) depicts the linear relationship between  $I_{\text{S}}/I_{\text{S0}}$  and  $C_{\text{S+A}}^{n/3}$ . An optimal linear behavior was obtained at  $n = 10$ , indicating that q-q interactions determined the mechanism of energy transfer between Ce<sup>3+</sup> and Eu<sup>2+</sup> ions.

Fig. 3(a) displays the thermal spectra of CSO:0.4% Ce<sup>3+</sup>, 0.1% Eu<sup>2+</sup>. The emission intensity reached 40.8% (398 K) of that at room temperature (298 K), which is 13.4% higher than that of CSO:0.4% Ce<sup>3+</sup>. To explore why thermal stability increased, Fig. 3(b) demonstrates the pyrothermal spectra of two samples before and after Ce<sup>3+</sup> doping. Obviously, the pyrothermal curve intensity for the sample doped only with Eu<sup>2+</sup> is nearly zero, indicating no trap. Conversely, after introducing isoivalent Ce<sup>3+</sup>, a peak appears in the pyroheat curve around 343 K. This suggests that blending Ce<sup>3+</sup>-Eu<sup>2+</sup> has created a shallow trap. The reason for occurrence of the trap was that the introduction of Ce<sup>3+</sup> destroyed the original charge balance of the matrix. In order to maintain the charge balance, two Ce<sup>3+</sup> replaced three Sr<sup>2+</sup> to creating one doubly negatively charged Sr vacancy ( $V_{\text{Sr}}''$ ) and two positively charged defects  $[\text{Ce}^{3+}]_{\text{Sr}}'$ . The substitution process was as follows.



The schematic of Ce<sup>3+</sup>-Eu<sup>2+</sup> energy transfer and thermal stability enhancement is given in Fig. 3(c). The electrons of Ce<sup>3+</sup> jumped from the 4f ground state to 5d energy level after getting excited by a 467 nm light. A part of the electrons returned to the 4f ground state *via* radiative leaps and produced a broadband



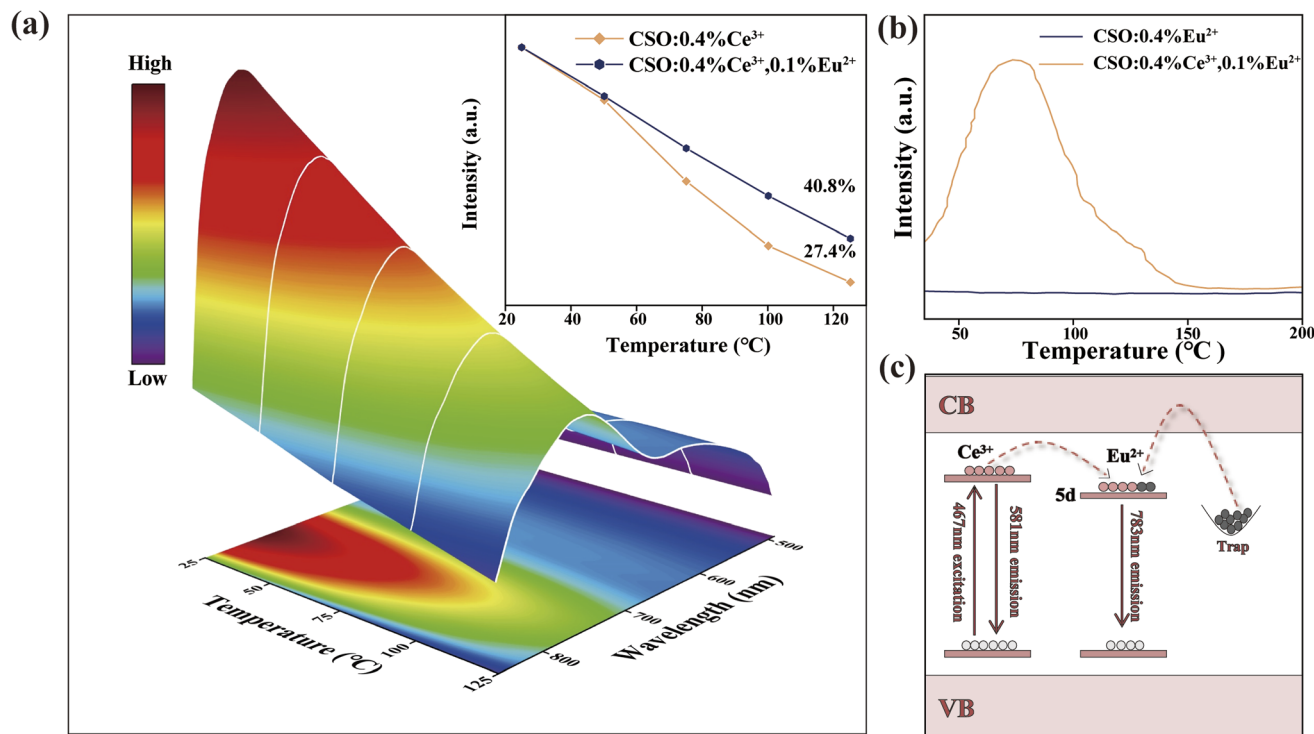


Fig. 3 (a) Temperature-dependent PL spectra of CSO:0.4% Ce<sup>3+</sup>,0.1% Eu<sup>2+</sup>, inset: intensities of CSO:0.4% Ce<sup>3+</sup> and CSO:0.4% Ce<sup>3+</sup>, 0.1% Eu<sup>2+</sup> at different temperatures; (b) TL curves of CSO:0.1% Eu<sup>2+</sup> and CSO:0.4% Ce<sup>3+</sup>, 0.1% Eu<sup>2+</sup>; and (c) mechanism diagram showing Ce<sup>3+</sup>–Eu<sup>2+</sup> energy transfer and thermal stability enhancement.

yellow luminescence, and another part of the electrons got transferred to the 5d energy level of Eu<sup>2+</sup> *via* energy transfer and returned to the 4f ground state *via* radiative leaps, producing a broadband NIR emission. In addition, a small fraction of electrons was trapped and stored therein. In luminescent materials, nonradiative transitions are mainly caused by factors such as lattice vibrations and defects. When the temperature increases, the lattice vibration intensifies, which makes it easier for the electrons to return from the excited state to the ground state, thus increasing the probability of non-radiative transitions. In addition, defects in the material can have a significant effect on the non-radiative transitions. The presence of defects disrupts the periodic potential field of the lattice, creating localized potential wells, in which the electrons undergo non-radiative leaps. In this study, we observed that when the temperature was increased, the electrons stored in the traps jumped out of the traps owing to thermal excitation and moved through the conduction band to the 5d energy level of Eu<sup>2+</sup>. This process effectively replaced a part of the electron loss due to the increased probability of nonradiative leaps as a result of temperature elevation, resulting in an improvement in the thermal stability of the sample. In addition, we experimentally measured the quantum efficiency of the system to be 45.8% (as shown in Fig. S2†). This result also reflected that the material was thermally stable to a certain extent, and it can effectively suppress the effect of nonradiative transitions on the luminescence performance, demonstrating more intuitively the effects

of lattice vibrations and defect changes on nonradiative transitions.

## 4. Application

Organic solutions contain a large number of chemical bonds such as C–H, C–O and O–H; these chemical bonds can absorb near infrared light of specific wavelengths, and accordingly, the concentration of the organic solvents can be detected using an NIR light. An NIR pc-LED was prepared by combining a blue LED with CSO:0.4% Ce<sup>3+</sup>, 0.1% Eu<sup>2+</sup> for concentration detection of ethanol (C<sub>2</sub>H<sub>5</sub>OH) solutions. Fig. 4(a) exhibits the experimental design for solution concentration detection. The NIR pc-LED emitted NIR light, which was passed through cuvettes with different concentrations of ethanol solution, and was finally received by the detector and presented on a computer in the form of a spectrum. Fig. 4(b) displays the experimental device. Fig. 4(c) exhibits the transmission spectra of the NIR pc-LED after passing through 0%, 20%, 40%, 60% and 80% ethanol solutions. It can be seen that as the concentration of the ethanol solution gradually increased, the absorption also gradually increased but the luminescence intensities gradually decreased. The intensity of the NIR light after passing through the ethanol solution and the concentration of the components in the sample complied with the Lambert–Beer law:

$$A = \log \frac{I_0}{I} = \epsilon bc, \quad (7)$$



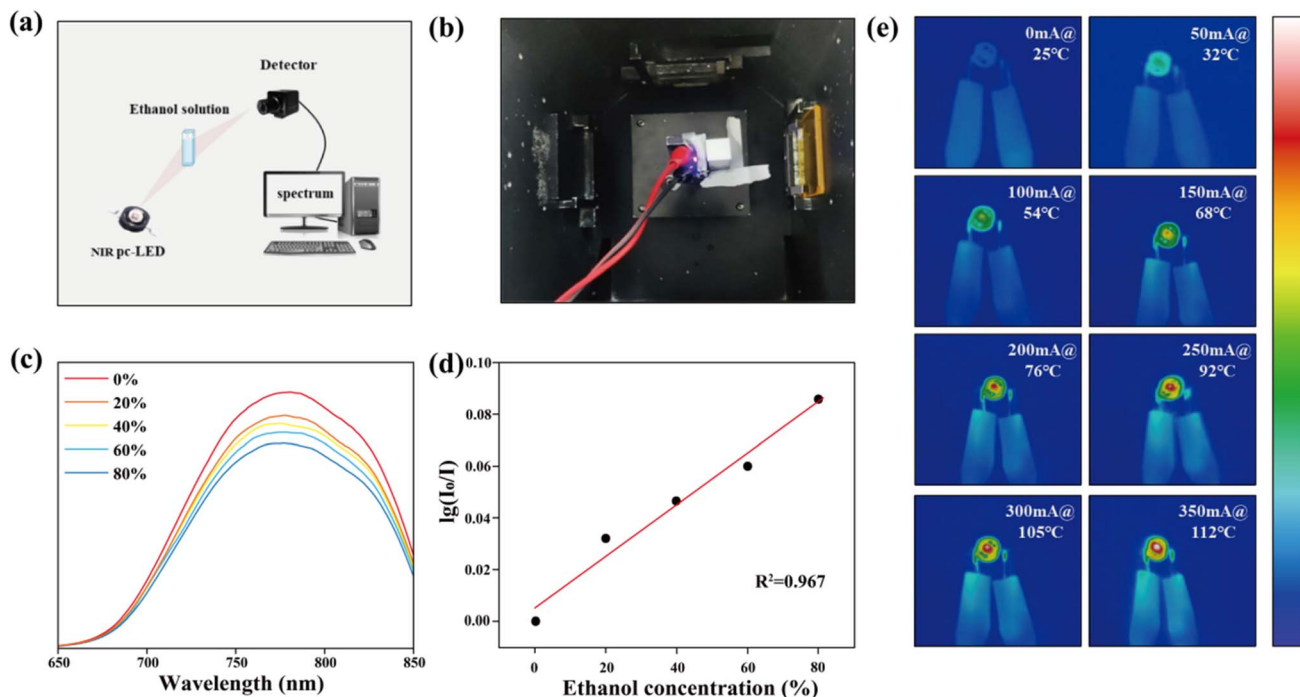


Fig. 4 (a) Schematic of the experimental design for solution concentration detection; (b) experimental device; (c) transmission spectra of the NIR pc-LED after passing through different concentrations of ethanol; (d) relationship between absorbance and concentration of ethanol solution; and (e) thermal images of the NIR pc-LED at different working currents ranging between 0–350 mA.

where  $A$  is the absorbance,  $I_0$  is the initial intensity,  $I$  is the intensity after passing through different concentrations of ethanol solutions,  $\epsilon$  denotes the molar absorptivity of the analyte,  $c$  is the concentration of the fraction to be tested, and  $b$  is the effective path length. The dependence of the luminescence intensity on the ethanol concentration was calculated. As illustrated in Fig. 4(d), the absorbance and ethanol concentration showed a good linear correlation after the fitting, and the fit reached  $R^2 = 0.967$ , indicating that the phosphor could offer a good application prospect in the field of concentration detection of solutions. The NIR pc-LED produced different amount of heat under different working currents, and thus, the temperature of the NIR pc-LED increased. Fig. 4(e) exhibits the pyrometer image of the NIR pc-LED under different working currents (0–350 mA). It can be seen that the temperature gradually increased with increasing working current, and when the working current reached 350 mA, the temperature reached 385 K.

## 5. Conclusions

In conclusion, the novel NIR phosphor  $\text{Ca}_{0.8}\text{Sr}_{0.2}\text{O}:\text{Eu}^{2+}$  was synthesized *via* a solid-state method. When  $\text{Ce}^{3+}$  ions were introduced, the luminescence performance of  $\text{Ca}_{0.8}\text{Sr}_{0.2}\text{O}:\text{Ce}^{3+}$ ,  $\text{Eu}^{2+}$  was obviously improved. Importantly, the quantum efficiency of  $\text{Ca}_{0.8}\text{Sr}_{0.2}\text{O}:\text{Eu}^{2+}$  increased from 36.7% to 45.8%, and the thermal stability at 398 K increased from 27.4% to 40.8%. The decay curves confirmed that the reason for this result was the occurrence of energy transfer between  $\text{Ce}^{3+}-\text{Eu}^{2+}$ . The NIR pc-LED prepared by combining  $\text{Ca}_{0.8}\text{Sr}_{0.2}\text{O}:\text{Eu}^{2+}$ ,

0.1%  $\text{Eu}^{2+}$  with a blue LED chip verified its promising application in the concentration detection of organic solutions.

## Data availability

All relevant data are within the manuscript and its ESI.†

## Conflicts of interest

The authors declare that they have no conflicts of interest.

## Acknowledgements

This work was supported by the National Natural Science Foundation of China (No. 51902080) and the Natural Science Foundation of Hebei Province, China (No. A2023201014).

## References

- 1 L. Zhang, H. Xu and M. Gu, Use of signal to noise ratio and area change rate of spectra to evaluate the visible/NIR spectral system for fruit internal quality detection, *J. Food Eng.*, 2014, **139**, 19–23.
- 2 A. Guelpa, F. Marini, A. du Plessis, R. Slabbert and M. Manley, Verification of authenticity and fraud detection in South African honey using NIR spectroscopy, *Food Control*, 2017, **73**, 1388–1396.
- 3 K. Deng, R. Y. Zhang, L. Yuan, H. Wu and Y. Hu, Luminescent properties of broad band far red emitting

- Zn<sub>3</sub>Ga<sub>2</sub>GeO<sub>8</sub>:Mn<sup>2+</sup>, Ca<sup>2+</sup> phosphors for indoor plant growth LED, *Appl. Phys. A: Mater. Sci. Process.*, 2023, **129**(1), 69–75.
- 4 A. Dalle Zotte, M. Ottavian, A. Concollato, L. Serva, R. Martelli and G. Parisi, Authentication of raw and cooked freeze-dried rainbow trout (*Oncorhynchus mykiss*) by means of near infrared spectroscopy and data fusion, *Food Res. Int.*, 2014, **60**, 180–188.
- 5 Q. Zhang, D. Liu, P. Dang, H. Lian, G. Li and J. Lin, Two selective sites control of Cr<sup>3+</sup>-doped ABO<sub>4</sub> phosphors for tuning ultra-broadband near-infrared photoluminescence and multi-applications, *Laser Photon. Rev.*, 2022, **16**(2), 2100459–2100464.
- 6 S. He, P. Li, Y. Ren, G. Wei, Y. Wang, Y. Yang, R. Li, J. Li, Y. Shi, X. Shi and Z. Wang, Near-infrared broadband ZnTa<sub>2</sub>O<sub>6</sub>:Cr<sup>3+</sup> phosphor for pc-LEDs and its application to nondestructive testing, *Inorg. Chem.*, 2022, **61**(29), 11284–11292.
- 7 X. Zou, X. Wang, H. Zhang, Y. Kang, X. Yang, X. Zhang, M. S. Molochev and B. Lei, A highly efficient and suitable spectral profile Cr<sup>3+</sup>-doped garnet near-infrared emitting phosphor for regulating photomorphogenesis of plants, *Chem. Eng. J.*, 2022, **428**, 132003–132011.
- 8 Y. Shi, Z. Wang, J. Peng, Y. Wang, S. He, J. Li, R. Li, G. Wei, Y. Yang and P. Li, Achieving the ultra-broadband near-infrared La<sub>3</sub>SnGa<sub>5</sub>O<sub>14</sub>:Cr<sup>3+</sup> phosphor via multiple lattice sites occupation for biological nondestructive detection and night-vision technology, *Mater. Today Adv.*, 2022, **16**, 100305–100312.
- 9 N. Yeh and J. P. Chung, High-brightness LEDs-Energy efficient lighting sources and their potential in indoor plant cultivation, *Renewable Sustainable Energy Rev.*, 2009, **13**(8), 2175–2180.
- 10 L. Zhang, S. Zhang, Z. Hao, X. Zhang, G. H. Pan, Y. Luo, H. Wu and J. Zhang, A high efficiency broad-band near-infrared Ca<sub>2</sub>LuZr<sub>2</sub>Al<sub>3</sub>O<sub>12</sub>:Cr<sup>3+</sup> garnet phosphor for blue LED chips, *J. Mater. Chem. C*, 2018, **6**(18), 4967–4976.
- 11 N. A. Mohd Aziz, N. Arsad, P. S. Menon, S. Shaari, Z. Md Yusof and A. R. Laili, An assessment study of absorption effect: LED vs tungsten halogen lamp for noninvasive glucose detection, *J. Innovative Opt. Health Sci.*, 2015, **8**(2), 1550013–1550017.
- 12 H. Zeng, T. Zhou, L. Wang and R. Xie, Two-site occupation for exploring ultra-broadband near-infrared phosphor-double-perovskite La<sub>2</sub>MgZrO<sub>6</sub>:Cr<sup>3+</sup>, *Chem. Mater.*, 2019, **31**(14), 5245–5253.
- 13 M. Ye, Z. Gao, Z. Li, Y. Yuan and T. Yue, Rapid detection of volatile compounds in apple wines using FT-NIR spectroscopy, *Food Chem.*, 2016, **190**, 701–708.
- 14 S. Sarkar, P. Le, J. Geng, Y. Liu, Z. Han, M. U. Zahid, D. Nall, Y. Youn, P. R. Selvin and A. M. Smith, Short-wave infrared quantum dots with compact sizes as molecular probes for fluorescence microscopy, *J. Am. Chem. Soc.*, 2020, **142**(7), 3449–3462.
- 15 A. Zabliūtė, S. Butkutė, A. Žukauskas, P. Vitta and A. Kareiva, Sol-gel synthesized far-red chromium-doped garnet phosphors for phosphor-conversion light-emitting diodes that meet the photomorphogenetic needs of plants, *Appl. Opt.*, 2014, **53**(5), 907–914.
- 16 X. Zhang, J. Xu, Z. Guo and M. Gong, Luminescence and energy transfer of dual-emitting solid solution phosphors (Ca, Sr)<sub>10</sub>Li(PO<sub>4</sub>)<sub>7</sub>:Ce<sup>3+</sup>, Mn<sup>2+</sup> for ratiometric temperature sensing, *Ind. Eng. Chem. Res.*, 2017, **56**(4), 890–898.
- 17 M. Li, J. Zhang, J. Han, Z. Qiu, W. Zhou, L. Yu, Z. Li and S. Lian, Changing Ce<sup>3+</sup> content and codoping Mn<sup>2+</sup> induced tunable emission and energy transfer in Ca<sub>2.5</sub>Sr<sub>0.5</sub>Al<sub>12</sub>O<sub>6</sub>:Ce<sup>3+</sup>, Mn<sup>2+</sup>, *Inorg. Chem.*, 2017, **56**(1), 241–251.
- 18 K. Li, H. Lian, M. Shang and J. Lin, A novel greenish yellow-orange red Ba<sub>3</sub>Y<sub>4</sub>O<sub>9</sub>:Bi<sup>3+</sup>, Eu<sup>3+</sup> phosphor with efficient energy transfer for UV-LEDs, *Dalton Trans.*, 2015, **44**(47), 20542–20550.
- 19 W. Lv, M. Jiao, Q. Zhao, B. Shao, W. Lü and H. You, Ba<sub>1.3</sub>Ca<sub>0.7</sub>SiO<sub>4</sub>:Eu<sup>2+</sup>, Mn<sup>2+</sup>: a promising single-phase, color-tunable phosphor for near-ultraviolet white-light-emitting diodes, *Inorg. Chem.*, 2014, **53**(20), 11007–11014.
- 20 M. Ding, M. Xu and D. Chen, A new non-contact self-calibrated optical thermometer based on Ce<sup>3+</sup> → Tb<sup>3+</sup> → Eu<sup>3+</sup> energy transfer process, *J. Alloys Compd.*, 2017, **713**, 236–247.
- 21 L. L. Wang, Q. L. Wang, X. Y. Xu, J. Z. Li, L. B. Gao, W. K. Kang, J. S. Shi and J. Wang, Energy transfer from Bi<sup>3+</sup> to Eu<sup>3+</sup> triggers exceptional long-wavelength excitation band in ZnWO<sub>4</sub>:Bi<sup>3+</sup>, Eu<sup>3+</sup> phosphors, *J. Mater. Chem. C*, 2013, **1**(48), 8033–8040.
- 22 G. P. R. L. Blasse, Energy transfer in oxidic phosphors, *Phys. Lett. A*, 1968, **28**(6), 444–445.
- 23 H. Zhou, Q. Wang and Y. Jin, Temperature dependence of energy transfer in tunable white light-emitting phosphor BaY<sub>2</sub>Si<sub>3</sub>O<sub>10</sub>:Bi<sup>3+</sup>, Eu<sup>3+</sup> for near UV LEDs, *J. Mater. Chem. C*, 2015, **3**(42), 11151–11162.
- 24 D. L. Dexter, A theory of sensitized luminescence in solids, *J. Chem. Phys.*, 1953, **21**(5), 836–850.
- 25 J. Cui, P. Li, L. Cao, X. Wang, Y. Yao, M. Zhang, M. Zheng, Z. Yang, H. Suo and Z. Wang, Achievement of broadband near-infrared phosphor Ca<sub>3</sub>Y<sub>2</sub>Ge<sub>3</sub>O<sub>12</sub>:Cr<sup>3+</sup>, Ce<sup>3+</sup> via energy transfer for food analysis, *J. Lumin.*, 2021, **237**, 118170–118176.

